J. Fluid Mech. (2021), *vol*. 927, A10, doi:10.1017/jfm.2021.728

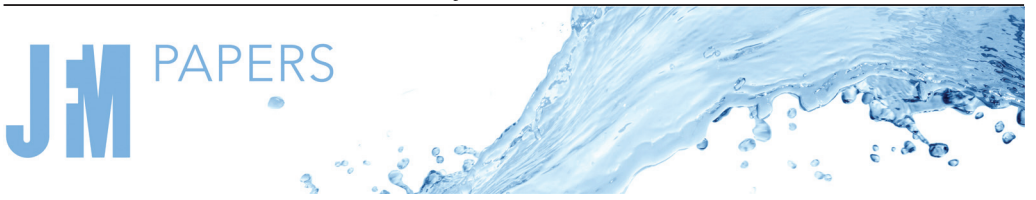

A reverse transition route from inertial to elasticity-dominated turbulence in viscoelastic Taylor–Couette flow

Jiaxing Song[1], Zhen-Hua Wan[1], Nansheng Liu[1,†], Xi-Yun Lu[1] and Bamin Khomami[2,†]

[1]Department of Modern Mechanics, University of Science and Technology of China, Hefei, Anhui 230026, PR China

[2]Department of Chemical and Biomolecular Engineering, University of Tennessee, Knoxville, TN 37996, USA

(Received 31 March 2021; revised 8 June 2021; accepted 12 August 2021)

A high-order transition route from inertial to elasticity-dominated turbulence (EDT) in Taylor–Couette flows of polymeric solutions has been discovered via direct numerical simulations. This novel two-step transition route is realized by enhancing the extensional viscosity and hoop stresses of the polymeric solution via increasing the maximum chain extension at a fixed polymer concentration. Specifically, in the first step inertial turbulence is stabilized to a laminar flow much like the modulated wavy vortex flow. The second step destabilizes this laminar flow state to EDT, i.e. a spatially smooth and temporally random flow with a -3.5 scaling law of the energy spectrum reminiscent of elastic turbulence. The flow states involved are distinctly different to those observed in the reverse transition route from inertial turbulence via a relaminarization of the flow to elasto-inertial turbulence in parallel shear flows, underscoring the importance of polymer-induced hoop stresses in realizing EDT that are absent in parallel shear flows.

Key words: viscoelasticity, transition to turbulence, Taylor–Couette flow

1. Introduction

Polymeric fluids are used to produce a huge variety of consumer products from household items to state-of-the-art composites used in applications of critical global needs (Denn 2004; Larson & Desai 2015; Benzi & Ching 2018). The nonlinear viscoelastic response of this class of fluids gives rise to a new class of instabilities and flow states that complicate liquid state processing of polymers. In fact, the strong coupling of inertial and elastic forces commonly quantified by the Reynolds (Re) and Weissenberg (Wi) numbers,

† Email addresses for correspondence: lns@ustc.edu.cn, bkhomami@utk.edu

respectively, leads to various flow transition routes to turbulent flow states that are specific to polymeric fluids (Morozov & van Saarloos 2007; Muller 2008; Dutcher & Muller 2013). A fascinating example is the elastically dominated inertialess flow state dubbed 'elastic turbulence' (ET) (Groisman & Steinberg 2000). Elastic turbulence displays large velocity fluctuations in a wide range of spatial and temporal scales with a power-law decay of the kinetic energy spectra in a frequency domain $E(k) \sim k^{-\alpha}$ with the exponent $\alpha > 3$ (between 3.3 and 3.6 depending on flow geometry) (Fouxon & Lebedev 2003; Steinberg 2019). Thus, due to the steep decay of the velocity spectrum, ET is essentially a spatially smooth and temporally random flow, dominated by a strong nonlinear interaction of a few large-scale spatial modes (Groisman & Steinberg 2004; Steinberg 2021).

In parallel shear flows, a full transition road map from inertial turbulence (IT) to a new turbulent-like regime dubbed elasto-inertial turbulence (EIT) has been discovered (Samanta *et al.* 2013; Choueiri, Lopez & Hof 2018; Lopez, Choueiri & Hof 2019; Shekar *et al.* 2019). Specifically, a reverse transition route from IT via a laminar base flow state to EIT is realized in pipe flows at a subcritical $Re \sim O(10^3)$ (Choueiri *et al.* 2018), whereupon enhancement of elastic forces either by increasing the polymer concentration and/or increasing Wi to $O(10)$, the flow first relaminarizes as the inertial quasi-streamwise vortices are gradually weakened and are finally eliminated (Choueiri *et al.* 2018; Lopez *et al.* 2019). This relaminarized state exhibits drag reduction beyond the maximum drag reduction asymptote (Toms 1948; Lumley 1969; Virk 1975) and subsequently undergoes a secondary instability, namely, elasto-inertial instability that results in a dominant flow structure consisting of two-dimensional sheets of highly stretched polymers in channel flows, and streamwise elongated streaks in pipe flows (Choueiri *et al.* 2018; Sid, Terrapon & Dubief 2018; Lopez *et al.* 2019; Shekar *et al.* 2019, 2020). The kinetic energy spectrum in the EIT regime has a $-14/3$ scaling, which is distinctly different from the Kolmogorov scaling of $-5/3$ for IT but close to the -3.5 scaling for ET (Fouxon & Lebedev 2003; Groisman & Steinberg 2004; Dubief, Terrapon & Soria 2013; Steinberg 2019). It should also be noted that another transition route towards EIT that bypasses the laminar state has been realized in pipe flows at a supercritical Re (Choueiri *et al.* 2018).

In curvilinear shear flows, our recent simulations (Liu & Khomami 2013*a*,*b*; Song *et al.* 2019) of the viscoelastic Taylor–Couette (TC) flows, i.e. the flows between two concentric, rotating cylinders (Taylor 1923), taken together with some preliminary experimental findings (Lee, Sengupta & Wei 1995; Dutcher & Muller 2011), are indicative of the existence of reverse transitions from IT to a new flow state that is more akin to ET than EIT. Specifically, at high levels of fluid elasticity, i.e. $Wi = 60$, the Newtonian turbulent Taylor vortex flow (TTV) at $Re = 3000$ and large radius ratio $\eta = R_i/R_o = 0.912$ is stabilized to a flow state resembling the Taylor vortex flow (TVF), where R_i and R_o are the inner and outer cylinder radii, respectively (Dutcher & Muller 2009; Song *et al.* 2019). In this transition the inertial small-scale Görtler vortices (GV) (Wei *et al.* 1992; Dong 2007) are eliminated; conversely, a similar Newtonian TTV at a small η (=0.5) transitions directly (without relaminarization) to an elasticity-dominated turbulence (EDT), as evidenced by destabilization of large-scale Taylor vortices (TV) via a hoop stress driven elastic/inertio-elastic Görtler instability that results in small near-wall turbulent vortices (Liu & Khomami 2013*b*; Song *et al.* 2019). A drastic drag enhancement (DE) is observed for these two very different, in fact nearly opposite, vortical changes. Evidently, the localized small-scale elastic structures in viscoelastic TC turbulence display streamwise-oriented flow topology, that are in stark contrast to the trains of weak spanwise-oriented flow structures with inclined sheets of polymer stretch in EIT of parallel shear flows. Hence, the underlying elasticity-driven physics and in particular

the role of hoop stresses in the generation of turbulence and vortical structures, DE, and the realization of a distinct flow state, namely EDT, remain an open question.

To this end, the viscoelastic TC flow is an ideal flow to examine the effects of polymeric elasticity mainly manifested through hoop stresses on flow transitions, pattern formations and turbulence dynamics (Groisman & Steinberg 1996, 1997, 1998*a*,*b*; Crumeyrolle & Mutabazi 2002; Dutcher & Muller 2011; Latrache, Crumeyrolle & Mutabazi 2012; Dutcher & Muller 2013). In what follows, we will demonstrate a novel transition route from IT to EDT in viscoelastic TC flow. This transition from a Newtonian TTV is facilitated by increasing the maximum chain extension (L) of the polymer additives that leads to a significant increase in hoop stresses that play a central role in determining flow patterns, dynamics and transitions. Specifically, the transition has three distinctive aspects: (1) dramatic DE; (2) a stabilization step that leads to a laminar flow much like the modulated wavy vortex flow (MWV); and (3) a subsequent destabilization of the laminar flow to an EDT regime with the hallmark signature of ET, i.e. a spatially smooth and temporally random flow with a -3.5 energy spectrum scaling. In turn, the underlying physical origin of this transition and the commensurate competition between inertial and elastic body forces are discussed.

2. Problem formulation and computational details

Direct numerical simulations using a fully spectral, three-dimensional parallel algorithm (Thomas *et al.* 2006*a*; Thomas, Khomami & Sureshkumar 2006*b*, 2009; Liu & Khomami 2013*a*,*b*; Song *et al.* 2019) have been performed to examine the flow dynamics in viscoelastic TC flow. We have chosen $d = R_o - R_i$, $d/(\Omega R_i)$, ΩR_i, $\rho(\Omega R_i)^2$ and $\eta_p \Omega R_i/d$ as scales for length, time, velocity $\boldsymbol{u}$, pressure P and polymer stress $\boldsymbol{\tau}$, respectively. Here Ω denotes the inner cylinder angular velocity, and ρ the solution density. The outer cylinder is considered to be stationary. The polymer stress $\boldsymbol{\tau}$ is related to the conformation tensor $\boldsymbol{C}$ through the finitely extensible nonlinear elastic-Peterlin (FENE-P) constitutive relation (Bird *et al.* 1987). The dimensionless governing equations for the incompressible flow of FENE-P fluid are

$$\boldsymbol{\nabla} \cdot \boldsymbol{u} = 0, \tag{2.1}$$

$$\frac{\partial \boldsymbol{u}}{\partial t} + \boldsymbol{u} \cdot \boldsymbol{\nabla} \boldsymbol{u} = -\boldsymbol{\nabla} P + \frac{\beta}{Re} \nabla^2 \boldsymbol{u} + \frac{1-\beta}{Re} \boldsymbol{\nabla} \cdot \boldsymbol{\tau} \tag{2.2}$$

and

$$\frac{\partial \boldsymbol{C}}{\partial t} + \boldsymbol{u} \cdot \boldsymbol{\nabla} \boldsymbol{C} = \boldsymbol{C} \cdot \boldsymbol{\nabla} \boldsymbol{u} + (\boldsymbol{\nabla} \boldsymbol{u})^{\mathrm{T}} \cdot \boldsymbol{C} - \boldsymbol{\tau} + \kappa \nabla^2 \boldsymbol{C}, \tag{2.3}$$

where polymer molecules are modelled as dumb-bells composed of two beads and a nonlinear spring, and the polymer stress $\boldsymbol{\tau}$ can be related to the stress conformation tensor $\boldsymbol{C}$ via the relationship

$$\boldsymbol{\tau} = \frac{f(\boldsymbol{C})\boldsymbol{C} - \boldsymbol{I}}{Wi}. \tag{2.4}$$

The function $f(\boldsymbol{C})$, known as the Peterlin function, is defined as

$$f(\boldsymbol{C}) = \frac{L^2 - 3}{L^2 - \mathrm{trace}(\boldsymbol{C})}, \tag{2.5}$$

where $Re = \rho \Omega R_i d/\eta_t$, with the total zero-shear viscosity η_t being the sum of the solvent (η_s) and polymeric (η_p) contributions; $Wi = \lambda \Omega R_i/d$, with λ being the elastic

relaxation time; and $\beta = \eta_s/\eta_t$. Here L is the maximum chain extensibility, in particular, the polymeric shear stress and normal stress (hoop stress) tend to increase at higher extensibilities, corresponding to the shear-thinning behaviour in both the shear viscosity and first normal stress coefficient (Ghanbari & Khomami 2014). The governing equations are supplemented by no-slip boundary conditions at walls, as well as periodic boundary conditions in the axial direction with a periodicity length of $4\pi d$. A small diffusive term $\kappa\nabla^2\boldsymbol{C}$ is added in the bulk flow region for numerical stabilization (Sureshkumar, Beris & Avgousti 1995, 1997). The original constitutive equation without the diffusive term is applied at the cylinder walls, hence, where boundary conditions for $\boldsymbol{C}$ are not imposed.

Inspired by previous simulations of EIT (Sid *et al.* 2018; Lopez *et al.* 2019; Shekar *et al.* 2019) and viscoelastic TC flow (Liu & Khomami 2013*a*,*b*; Song *et al.* 2019), we pursue a transition route from IT to EDT in a small gap viscoelastic TC flow system of $\eta = R_i/R_o = 0.912$, $Re = 3000$, $Wi = 60$ and $\beta = 0.8$, by enhancing the extensional viscosity and hoop stresses via increasing L from 30 to 240. The L values considered correspond to an extensibility number ($E_x = 2L^2(1-\beta)/3\beta$) ranging from 150 to 9600 (Xi & Graham 2010; Lopez *et al.* 2019). Based on our previous calculations (Song *et al.* 2019), for $L \leqslant 120$ a Schmidt number $Sc\,[\equiv (Re\kappa)^{-1}]$ of 0.42 is used with a mesh size of $128 \times 256 \times 256$ in the $r \times \theta \times z$ directions and a time step of 0.005; in order to reliably capture the polymer stress field at $L \geqslant 130$ a larger Sc (=0.83) is used along with a larger mesh size of $128 \times 256 \times 512$ and a smaller time step of 0.001. Simulation with finite Sc could modify the reported flow transitions; however, the spatial resolution and the Sc number used in this study are large enough to nearly quantitatively capture the essential flow features. Evidently, the choice of β affects the critical L for transition to elasticity-dominated flow as well as the onset of numerical instability. Nevertheless, the reported results not only capture the essential flow dynamics but also provide mechanistic insight for the novel reverse flow transitions observed in the viscoelastic TC flow. All the simulations for the viscoelastic TC flow are initiated from the Newtonian TTV state (Dutcher & Muller 2009). Sufficiently long simulations [typically of $\sim 300T$, $T = d/(\Omega R_i)$] are executed to ensure that statistically steady flow states have been realized. Moreover, ensemble averages are obtained over a time period of $\sim 120T$.

3. Results and discussion

Our results indicate a novel flow transition route from IT to EDT that contains a stabilization step ($L = 30 \sim 120$) and a subsequent destabilization step ($L = 130 \sim 240$), as evidenced by the vortical changes depicted in figures 1 and 2. Similar to our previous findings (Liu & Khomami 2013*b*; Song *et al.* 2019), these transitions lead to a dramatic DE, namely, from 24 % to 81 % in the stabilization step and from 50 % to 138 % in the destabilization step, as shown in table 1. The angular momentum current J^ω in viscoelastic turbulent TC flow is defined as (Song *et al.* 2019)

$$J^\omega = r^3[\langle u_r\omega\rangle - \beta\partial_r\langle\omega\rangle/Re - (1-\beta)\langle\tau_{r\theta}\rangle/r/Re]. \tag{3.1}$$

Hereafter, $\langle\,\rangle$ denotes ensemble averaging in time, the θ- and z-directions. Here $\omega = u_\theta/r$ denotes the angular velocity. The right-hand terms of (3.1) represent in sequence the contributions of convective flux (J_c^ω), the diffusive flux (J_d^ω) and the elastic source/sink term (J_p^ω) to the angular momentum (Song *et al.* 2019). The Nusselt number is calculated as $Nu_\omega = J^\omega/J^\omega_{lam}$, with J^ω_{lam} being the Newtonian laminar value; hence, J_c^ω/J^ω represents the inertia contribution to Nu_ω, i.e. convection mainly arising from the large-scale TV, and J_p^ω/J^ω represents the elastic contribution. As shown in figures 1(*a*) and 2(*a*),

L	0	30	60	100	120	130	140	160	200	240
Nu_ω	4.57	5.66	6.93	7.88	8.28	6.85	7.76	8.49	9.89	10.88
J_c^ω/J^ω	98 %	85 %	94 %	126 %	116 %	107 %	91 %	78 %	46 %	31 %
J_p^ω/J^ω	0 %	15 %	8 %	−22 %	−14 %	−6 %	9 %	24 %	54 %	68 %
DE	0 %	24 %	52 %	72 %	81 %	50 %	70 %	86 %	116 %	138 %

Table 1. Nusselt number $Nu_\omega = J^\omega/J^\omega_{lam}$ where J^ω is the angular momentum current defined in (3.1) and J^ω_{lam} is its Newtonian laminar flow counterpart, convective flux (J^ω_c) and polymeric elastic source/sink (J^ω_p) contribution to the angular momentum J^ω of TC flows at the middle of the gap for various L. Here $L = 0$ corresponds to the Newtonian TTV flow; DE is calculated as $(Nu_\omega - Nu_\omega^{L=0})/Nu_\omega^{L=0}$.

the Newtonian TTV regime can be viewed as a superimposition of near-wall small-scale GV on the large-scale TV that occupy the entire gap (Dutcher & Muller 2009). To be more specific, as fluid inertia is enhanced gradually, the TTV is realized via a sequence of flow transitions from circular Couette flow, to axially periodic TVF, and then subsequently to wavy vortex flow (known as WVF), MWV, chaotic wavy vortex (CWV) flow, wavy turbulent vortex (WTV) flow and finally to TTV flow (Dutcher & Muller 2009). In the TTV regime, the large-scale TV are highly oscillatory in time, as evidenced by their fluctuating boundaries, i.e. the inflow (blue) and outflow (red) stripes (see figure 1*a*). The spatial small-scale fluid motions are ascribed to the inertial small-scale GV that lead to high-intermittency oscillations of the large-scale TV (see figure 2*a*). The dominant spatial mode for this flow regime is $k_0 = 5$ and the energy spectrum has a $-5/3$ scaling signifying its IT origin (see figure 3*a*).

Evidently, the stabilized flow is characterized by a gradual elimination of the inertial small-scale GV and stabilization of the large-scale TV. Specifically, when polymer additives with $L = 30$ are introduced, the small-scale GV are greatly weakened (see figure 2*b*) and consequently, the large-scale TV exhibit temporally random wavy oscillations (see figure 1*b*) resulting in a weakly turbulent flow, namely, the WTV flow regime (Dutcher & Muller 2009). For $L = 60$, the disordered wavy oscillations of the large-scale TV become weaker (see figure 1*c*) as the near-wall small-scale GV are almost eliminated (see figure 2*c*). This is reminiscent of the Newtonian CWV flow regime (Dutcher & Muller 2009). Further increase in L to 120 relaminarizes the viscoelastic TC flow to a MWV-like laminar flow that has trivial interactions between two neighbouring stabilized large-scale TV, as evidenced by the small temporal variations of large-scale TV boundaries (see figures 1*d* and 2*d*). This stabilization step is qualitatively opposite to the classic inertially driven transition sequence, namely, from TVF to MWV, CWV, WTV and finally to TTV (Dutcher & Muller 2009). Spectral changes as L is enhanced are shown in figure 3(*a*), namely, drastic decrease of small scales by several orders and increased dominance of the primary spatial mode ($k_0 = 5$) and its superharmonics.

The subsequent destabilized flows result from the nonlinear interactions of the large-scale TV which become unstable as L is increased over 130. These interactions are manifested as a complex combination of merging and splitting along with oscillating of the large-scale TV (see figures 1 and 2), much like the experimental observations of the so-called merge–split transition to EIT in viscoelastic TC flow of $Re \sim O(10^2)$ (Cagney, Lacassagne & Balabani 2020; Lacassagne *et al.* 2020). Specifically, vortex merging and splitting events (VMSE) trigger a nonlinear transition to a chaotic regime dubbed elasticity-dominated chaotic flow (EDC) for $L = 130$ and 160 (see figures 1*e*,*f* and 2*e*,*f*). In the EDC, the large-scale TV are stable with a lifetime of $>30T$, and have

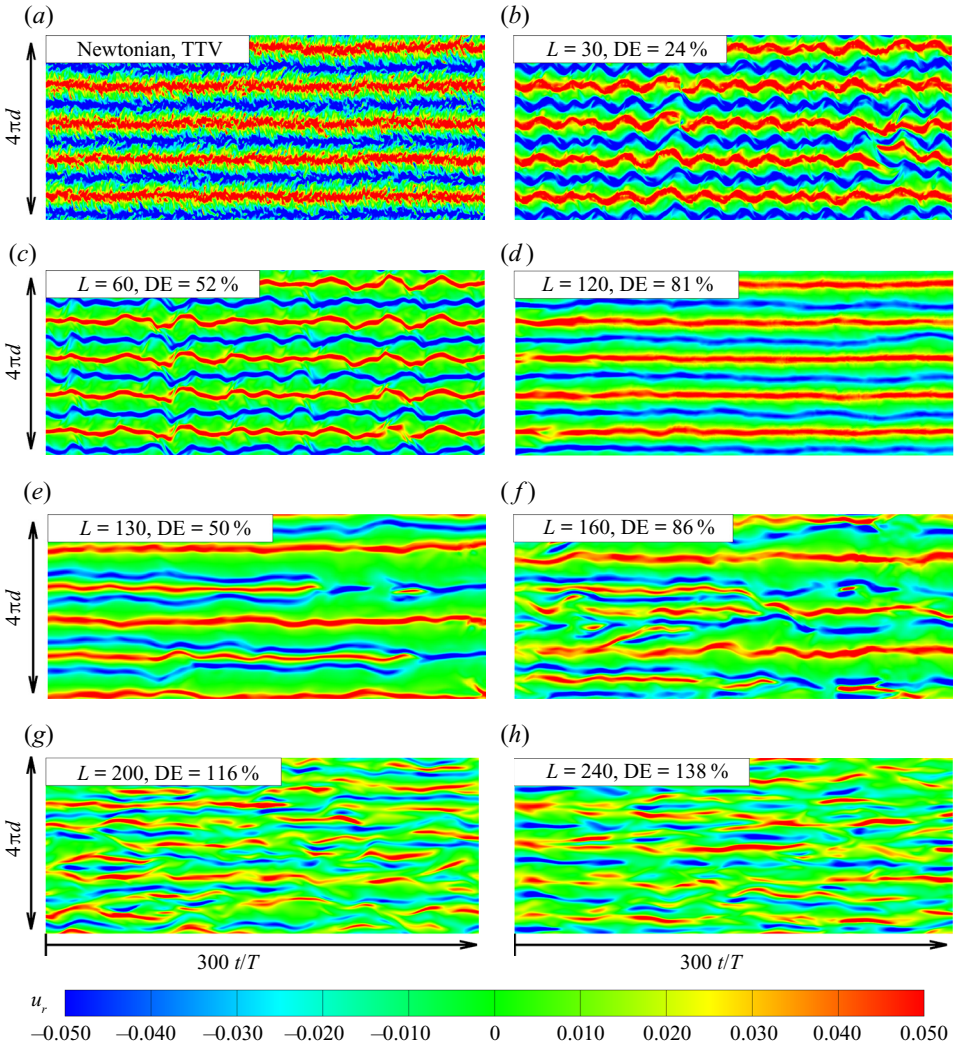

Figure 1. Space–time plots of radial velocity u_r obtained along the axial line at $r = (R_i + R_o)/2$ and $\theta = \pi$ for (*a*) Newtonian TTV, (*b*) $L = 30$, (*c*) $L = 60$, (*d*) $L = 120$, (*e*) $L = 130$, (*f*) $L = 160$, (*g*) $L = 200$, (*h*) $L = 240$. The blue and red contour regions correspond to the radial inflows ($u_r < 0$) and outflows ($u_r > 0$), respectively.

relatively larger axial sizes corresponding to a dominant spatial mode $k_0 = 3$ and 4 for $L = 130$ and 160, respectively (see figure 3*b*). The flow approaches the EDT regime for $L = 200$ and 240, which is characterized by a highly intermittent occurrence of the VMSE and the notably distorted large-scale TV (see figures 1*g*,*h* and 2*g*,*h*). In contrast, no dominant spatial mode is identified for the EDT (see figure 3*b*), and remarkably, a -3.5 spectral scaling is observed for these two regimes, thus justifying the designation of EDC and EDT. Recently, experimental studies on the elasto-inertial transitions in TC flow of viscoelastic polymer solutions have shown that shear-thinning acts to suppress elastic instabilities in the viscoelastic TC flows (Lacassagne, Cagney & Balabani 2021). The simulation results here support this argument, i.e. elasticity-dominated turbulent flow occurs at high L values where shear thinning effects are minimal but the driving force for instability and flow transition, namely hoop stresses and elongational viscosity,

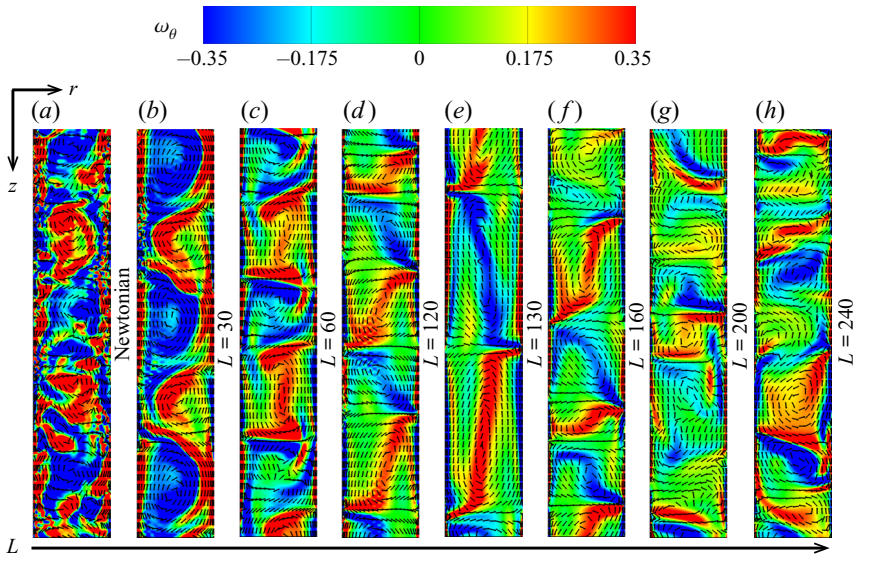

Figure 2. Instantaneous vectors of radial (u_r) and axial (u_z) velocities and contour plots of streamwise vorticity ω_θ in (r, z) plane with $\theta = \pi/2$, $0 \leqslant z \leqslant 2\pi d$ and $R_i \leqslant r \leqslant R_o$.

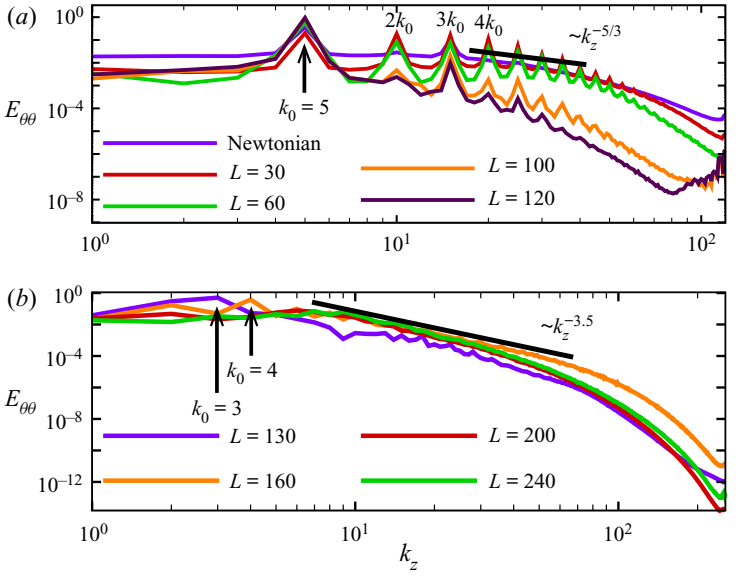

Figure 3. One-dimensional spectra of the streamwise turbulent kinetic energy ($\langle u'_\theta u'_\theta \rangle$) for ($a$) the stabilization step and (b) the destabilization step, where the azimuthal velocity fluctuation u'_θ is sampled at the middle of the gap. Hereafter, the fluctuating velocity $\boldsymbol{u}'$ is obtained as $\boldsymbol{u}' = \boldsymbol{u} - \langle \boldsymbol{u} \rangle$.

are large. Similar to inertialess ET (Groisman & Steinberg 2000, 2004; Steinberg 2021), these two flow regimes are spatially smooth and temporally random and the flow dynamics are dominated by the VMSE of oscillating large-scale TV. This points to the universality of flow-microstructure coupling and energy spectra in elastically dominated flows over a broad range of *Re*. Hence, the spatial small-scale fluid motions are originated by VMSE

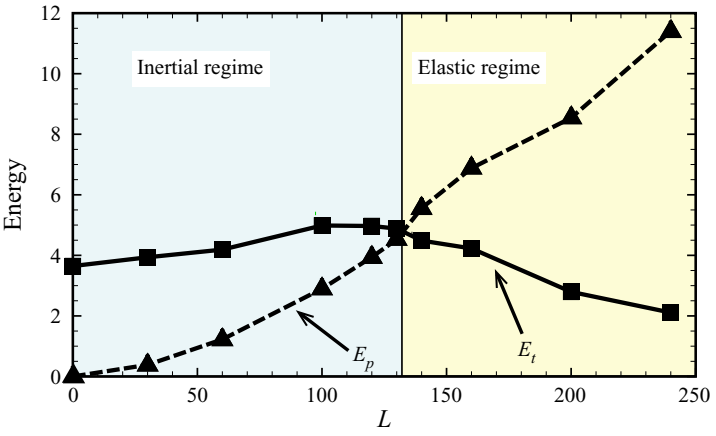

Figure 4. Total turbulent kinetic energy E_t and elastic potential energy E_p of viscoelastic TC flow for various L; $L = 0$ corresponds to the Newtonian TTV flow. Here $E_t = 8\pi^2\,\mathrm{d}\int_{R_i}^{R_o}\langle \boldsymbol{u}'^2\rangle/2r\,\mathrm{d}r$ and $E_p = 8\pi^2\,\mathrm{d}\int_{R_i}^{R_o}(1-\beta)(L^2-3)\langle \ln(f(\boldsymbol{C}))\rangle/(2ReWi)r\,\mathrm{d}r$.

via the resulting chaotic variations of polymer stresses at smaller scales (Groisman & Steinberg 2000, 2004; Steinberg 2021).

The intricate competition between inertial and elastic nonlinearities underlying this transition route is substantiated in figure 4 via the changes in total turbulent kinetic energy (E_t) and elastic potential energy (E_p). Note that, E_t is calculated by the fluctuating velocity $\boldsymbol{u}'$ that results from the large-scale TV oscillations and the small-scale turbulent motions, and thus can be viewed as a proper dynamical measure of inertial nonlinearity. Evidently, the stabilization step has a slight increase in E_t followed by a more pronounced decrease in the destabilization step. For $L < 130$, E_t is much larger than E_p. However, E_p becomes larger than E_t after the onset of EDC at $L = 130$ and increases continuously as L is increased. This clearly demonstrates that the nonlinear flow dynamics are inertia-dominated and then elasticity-dominated in the stabilized and destabilized flows, respectively. This is consistent with the above findings that the EDC and EDT are essentially of elastic origin as the inertial small-scale GV are fully eliminated.

The classic Pakdel–McKinley (PM) criterion (McKinley, Pakdel & Oeztekin 1996; Pakdel & McKinley 1996) for identification of the primary elastic instability in curvilinear flows (Larson, Shaqfeh & Muller 1990; Larson 1992; Sureshkumar, Beris & Avgousti 1994; Shaqfeh 1996; Groisman & Steinberg 1998*b*; Al-Mubaiyedh, Sureshkumar & Khomami 1999, 2000, 2002) should provide insight on flow destabilization observed in this study. The extended version of this criterion for viscoelastic TC flow with negligible inertia is given by (Schäfer, Morozov & Wagner 2018)

$$\sqrt{\epsilon}Wi^{rheo} \geqslant \frac{M_{crit}}{\sqrt{2}}\sqrt{1-\beta}\sqrt{1+\frac{3}{2}\epsilon+\frac{\epsilon^2}{2(\epsilon+2)}}, \tag{3.2}$$

where $\epsilon = d/R_i$ is the curvature, $Wi^{rheo} = N_1/(2|\Sigma_{r\theta}|)$ is the rheological Weissenberg number defined by the ratio of first normal stress difference $N_1 = \tau_{\theta\theta} - \tau_{rr}$ and the total shear stress $\Sigma_{r\theta}$ that herein has an inertial part across the gap, i.e. the Reynolds stress $\langle u_r' u_\theta'\rangle$ (Song *et al.* 2019), since high-*Re* viscoelastic TC flows are considered in the present study; $M_{crit} \approx 1.8$ is the instability threshold obtained experimentally that corresponds

L	30	60	100	120	130	140	160	200	240
$\sqrt{\epsilon}Wi^{rheo}$	0.2	0.49	1.07	1.34	1.36	1.52	1.62	2.20	2.53
$\sqrt{\epsilon}Wi^{eff}$	0.064	0.170	0.361	0.545	0.669	0.741	0.793	1.064	1.284

Table 2. Minimum values of ensemble-averaged instability onset condition across the gap for various L.

to the instability condition $\sqrt{\epsilon}Wi^{rheo} \approx 0.61$ for onset of the elastic instability (Schäfer *et al.* 2018). Evidently, $\sqrt{\epsilon}Wi^{rheo}$ is flow and geometry dependent and thus can serve as a dynamic indicator for the coupled inertial and elastic nonlinearities in curvilinear flows. However, this criterion does not explicitly take into account finite extensibility of the polymer chain, quantified by L in the FENE-P model. It is clear that the value of L plays an important role in both polymer induced flow transitions and drag modifications. Motivated by this fact, Li, Sureshkumar & Khomami (2015), in their study of polymer induced drag reduction in channel flows, developed an effective Weissenberg number for the FENE-P model ($Wi^{eff} = Wi^{rheo}[1 - \mathrm{tr}(\boldsymbol{C})/L^2]$) to more accurately capture flow microstructure coupling in the extensionally dominated regions of the flow, i.e. the biaxial extensional flow between streaks. To this end, we have changed the 'rheological Weissenberg number' Wi^{rheo} as the effective Weissenberg number Wi^{eff} in the extended PM criterion. In turn, the instability onset condition, i.e. $\sqrt{\epsilon}Wi^{eff}$, has been determined based on this criterion (see table 2). It should be noted that Wi^{rheo} and Wi^{eff} are functions of the radial position. Specifically, they have nearly equivalent maximum values near both cylinder walls and their respective minimum values occur at the middle of the gap. Hence, values at the middle of the gap are used to determine the critical onset condition for the instability. Using this new criterion, i.e. $\sqrt{\epsilon}Wi^{eff}$, the onset condition for instability monotonically increases as L is increased and becomes larger than the critical value of 0.61 suggested by Schäfer *et al.* (2018) at $L = 130$, which corresponds to direct numerical simulation predictions of the onset of elasticity-dominated flows. Thus, this new PM criterion not only provides much more reasonable values for the onset condition of the elastic instability, but also correctly captures the changes in this condition as L is enhanced, even at relatively high Re.

4. Conclusions

In summary, a complete transition route from IT to EDT has been numerically realized for the first time in the viscoelastic TC flow. This transition route that leads to significant DE is composed of a first stabilization step that gives rise to a MWV-like laminar regime, followed by a destabilization step that gives rise to EDT that has the hallmark signatures of ET. Taken together with another L-driven transition in a large gap viscoelastic TC flow with $\eta = 0.5$ (Liu & Khomami 2013*b*) from IT to EDT where the laminar state is bypassed, it paves the way for developing a full transition road map from IT to EDT in curvilinear wall bounded shear flows. Despite distinct differences in coherent structures and turbulent friction drag between EDT in TC flow and EIT in parallel shear flows, they have similar turbulent energy spectra. This points to the universality of elastically driven turbulent flow of dilute polymeric solutions, irrespective of the origin of elastic body forces. To this end, a solid foundation for research on polymer-induced transitions in high and low Re shear flows focused on detailed mechanistic understanding of EDT and ET and existence of spectral universality in this class of flows has been developed.

Acknowledgements. The calculations were completed on the supercomputing system in the Supercomputing Center at the University of Science and Technology of China.

Funding. This work was supported by the National Natural Science Foundation of China (J.S., Z.W., N.L. and X.L. grant numbers 12172353, 92052301, 12172351, 11621202, 11572312), the Science Challenge Project (N.L. and X.L. grant number TZ2016001), the National Science Foundation (B.K. grant number CBET0755269) and the Fundamental Research Funds for the Central Universities and the USTC Research Funds of the Double First-Class Initiative (Z.W.).

Declaration of interests. The authors report no conflict of interest.

Author ORCIDs.
- Jiaxing Song https://orcid.org/0000-0002-9341-0345;
- Zhen-Hua Wan https://orcid.org/0000-0003-0035-3116;
- Nansheng Liu https://orcid.org/0000-0001-9128-1933;
- Xi-Yun Lu https://orcid.org/0000-0002-0737-6460;
- Bamin Khomami https://orcid.org/0000-0002-0091-2312.

References

Al-Mubaiyedh, U.A., Sureshkumar, R. & Khomami, B. 1999 Influence of energetics on the stability of viscoelastic Taylor–Couette flow. *Phys. Fluids* **11**, 3217–3226.

Al-Mubaiyedh, U.A., Sureshkumar, R. & Khomami, B. 2000 Linear stability of Taylor–Couette flow: influence of fluid rheology and energetics. *J. Rheol.* **44**, 1121–1138.

Al-Mubaiyedh, U.A., Sureshkumar, R. & Khomami, B. 2002 The effect of viscous heating on the stability of Taylor–Couette flow. *J. Fluid Mech.* **462**, 111–132.

Benzi, R. & Ching, E.S.C. 2018 Polymers in fluid flows. *Annu. Rev. Condens. Matter Phys.* **9**, 163–181.

Bird, R.B., Curtiss, C.F., Armstrong, R.C. & Hassager, O. 1987 Kinetic theory. In *Dynamics of Polymeric Fluids*, pp. 1397–1398. Wiley.

Cagney, N., Lacassagne, T. & Balabani, S. 2020 Taylor–Couette flow of polymer solutions with shear-thinning and viscoelastic rheology. *J. Fluid Mech.* **905**, A28.

Choueiri, G.H., Lopez, J.M. & Hof, B. 2018 Exceeding the asymptotic limit of polymer drag reduction. *Phys. Rev. Lett.* **120**, 124501.

Crumeyrolle, O. & Mutabazi, I. 2002 Experimental study of inertio-elastic Couette–Taylor instability modes in dilute and semidilute polymer solutions. *Phys. Fluids* **14**, 1681–1688.

Denn, M.M. 2004 Fifty years of non-Newtonian fluid dynamics. *AIChE J.* **50**, 2335–2345.

Dong, S. 2007 Direct numerical simulation of turbulent Taylor–Couette flow. *J. Fluid Mech.* **587**, 373–393.

Dubief, Y., Terrapon, V.E. & Soria, J. 2013 On the mechanism of elasto-inertial turbulence. *Phys. Fluids* **25**, 110817.

Dutcher, C.S. & Muller, S.J. 2009 Spatio-temporal mode dynamics and higher order transitions in high aspect ratio Newtonian Taylor–Couette flows. *J. Fluid Mech.* **641**, 85–113.

Dutcher, C.S. & Muller, S.J. 2011 Effects of weak elasticity on the stability of high Reynolds number co- and counter-rotating Taylor–Couette flows. *J. Rheol.* **55**, 1271–1295.

Dutcher, C.S. & Muller, S.J. 2013 Effects of moderate elasticity on the stability of co- and counter-rotating Taylor–Couette flows. *J. Rheol.* **57**, 791–812.

Fouxon, A. & Lebedev, V. 2003 Spectra of turbulence in dilute polymer solutions. *Phys. Fluids* **15**, 2060–2072.

Ghanbari, R. & Khomami, B. 2014 The onset of purely elastic and thermo-elastic instabilities in Taylor–Couette flow: influence of gap ratio and fluid thermal sensitivity. *J. Non-Newtonian Fluid Mech.* **208–209**, 108–117.

Groisman, A. & Steinberg, V. 1996 Couette–Taylor flow in a dilute polymer solution. *Phys. Rev. Lett.* **77**, 1480–1483.

Groisman, A. & Steinberg, V. 1997 Solitary vortex pairs in viscoelastic Couette flow. *Phys. Rev. Lett.* **78**, 1460–1463.

Groisman, A. & Steinberg, V. 1998*a* Elastic vs inertial instability in a polymer solution flow. *Europhys. Lett.* **43**, 165–170.

Groisman, A. & Steinberg, V. 1998*b* Mechanism of elastic instability in Couette flow of polymer solutions: experiment. *Phys. Fluids* **10**, 2451–2463.

GROISMAN, A. & STEINBERG, V. 2000 Elastic turbulence in a polymer solution flow. *Nature* **405**, 53–55.
GROISMAN, A. & STEINBERG, V. 2004 Elastic turbulence in curvilinear flows of polymer solutions. *New J. Phys.* **6**, 29.
LACASSAGNE, T., CAGNEY, N. & BALABANI, S. 2021 Shear-thinning mediation of elasto-inertial Taylor–Couette flow. *J. Fluid Mech.* **915**, A91.
LACASSAGNE, T., CAGNEY, N., GILLISSEN, J.J.J. & BALABANI, S. 2020 Vortex merging and splitting: a route to elastoinertial turbulence in Taylor–Couette flow. *Phys. Rev. Fluids* **5** (1), 113303.
LARSON, R.G. 1992 Instabilities in viscoelastic flows. *Rheol. Acta* **31**, 213–263.
LARSON, R.G. & DESAI, P.S. 2015 Modeling the rheology of polymer melts and solutions. *Annu. Rev. Fluid Mech.* **47**, 47–65.
LARSON, R.G., SHAQFEH, E.S.G. & MULLER, S.J. 1990 A purely elastic transition in Taylor–Couette flow. *J. Fluid Mech.* **218**, 573–600.
LATRACHE, N., CRUMEYROLLE, O. & MUTABAZI, I. 2012 Transition to turbulence in a flow of a shear-thinning viscoelastic solution in a Taylor–Couette cell. *Phys. Rev.* E **86**, 056305.
LEE, S.H.K., SENGUPTA, S. & WEI, T. 1995 Effect of polymer additives on Görtler vortices in Taylor–Couette flow. *J. Fluid Mech.* **282**, 115–129.
LI, C.-F., SURESHKUMAR, R. & KHOMAMI, B. 2015 Simple framework for understanding the universality of the maximum drag reduction asymptote in turbulent flow of polymer solutions. *Phys. Rev.* E **92**, 043014.
LIU, N.S. & KHOMAMI, B. 2013*a* Elastically induced turbulence in Taylor–Couette flow: direct numerical simulation and mechanistic insight. *J. Fluid Mech.* **737**, R4.
LIU, N.S. & KHOMAMI, B. 2013*b* Polymer-induced drag enhancement in turbulent Taylor–Couette flows: direct numerical simulations and mechanistic insight. *Phys. Rev. Lett.* **111**, 114501.
LOPEZ, J.M., CHOUEIRI, G.H. & HOF, B. 2019 Dynamics of viscoelastic pipe flow at low Reynolds numbers in the maximum drag reduction limit. *J. Fluid Mech.* **874**, 699–719.
LUMLEY, J.L. 1969 Drag reduction by additives. *Annu. Rev. Fluid Mech.* **1**, 367–384.
MCKINLEY, G.H., PAKDEL, P. & OEZTEKIN, A. 1996 Rheological and geometric scaling of purely elastic flow instabilities. *J. Non-Newtonian Fluid Mech.* **67**, 19–47.
MOROZOV, A.N. & VAN SAARLOOS, W. 2007 An introductory essay on subcritical instabilities and the transition to turbulence in visco-elastic parallel shear flows. *Phys. Rep.* **447**, 112–143.
MULLER, S.J. 2008 Elastically-influenced instabilities in Taylor–Couette and other flows with curved streamlines: a review. *Korea-Aust. Rheol. J* **20**, 117–125.
PAKDEL, P. & MCKINLEY, G.H. 1996 Elastic instability and curved streamlines. *Phys. Rev. Lett.* **2459**, 12.
SAMANTA, D., DUBIEF, Y., HOLZNERA, M., SCHÄFER, C., MOROZOV, A.N., WAGNER, C. & HOF, B. 2013 Elasto-inertial turbulence. *Proc. Natl Acad. Sci. USA* **110**, 10557–10562.
SCHÄFER, C., MOROZOV, A. & WAGNER, C. 2018 Geometric scaling of elastic instabilities in the Taylor–Couette geometry: a theoretical, experimental and numerical study. *J. Non-Newtonian Fluid Mech.* **259**, 78–90.
SHAQFEH, E.S.G. 1996 Purely elastic instabilities in viscometric flows. *Annu. Rev. Fluid Mech.* **28**, 129–185.
SHEKAR, A., MCMULLEN, R.M., MCKEON, B.J. & GRAHAM, M.D. 2020 Self-sustained elastoinertial Tollmien–Schlichting waves. *J. Fluid Mech.* **897**, A3, 1–16.
SHEKAR, A., MCMULLEN, R.M., WANG, S., MCKEON, B.J. & GRAHAM, M.D. 2019 Critical-layer structures and mechanisms in elastoinertial turbulence. *Phys. Rev. Lett.* **122**, 124503.
SID, S., TERRAPON, V.E. & DUBIEF, Y. 2018 Two-dimensional dynamics of elasto-inertial turbulence and its role in polymer drag reduction. *Phys. Rev. Fluids* **3** (1), 011301.
SONG, J., TENG, H., LIU, N., DING, H., LU, X.-Y. & KHOMAMI, B. 2019 The correspondence between drag enhancement and vortical structures in turbulent Taylor–Couette flows with polymer additives: a study of curvature dependence. *J. Fluid Mech.* **881**, 602–616.
STEINBERG, V. 2019 Scaling relations in elastic turbulence. *Phys. Rev. Lett.* **123**, 234501–234505.
STEINBERG, V. 2021 Elastic turbulence: an experimental view on inertialess random flow. *Annu. Rev. Fluid Mech.* **53**, 27–58.
SURESHKUMAR, R., BERIS, A.N. & AVGOUSTI, M. 1994 Non-axisymmetric subcritical bifurcations in viscoelastic Taylor–Couette flow. *Proc. R. Soc. Lond.* A **447**, 135–153.
SURESHKUMAR, R., BERIS, A.N. & AVGOUSTI, M. 1995 Effect of artificial stress diffusivity on the stability of numerical calculations and the dynamics of time-dependent viscoelastic flows. *J. Non-Newtonian Fluid Mech.* **60**, 53–80.
SURESHKUMAR, R., BERIS, A.N. & AVGOUSTI, M. 1997 Direct numerical simulation of the turbulent channel flow of a polymer solution. *Phys. Fluids* **9**, 743–755.
TAYLOR, G.I. 1923 Stability of a viscous liquid contained between two rotating cylinders. *Phil. Trans. R. Soc. Lond.* A **223**, 289.

THOMAS, D.G., AL-MUBAIYEDH, U.A., SURESHKUMAR, R. & KHOMAMI, B. 2006*a* Time dependent simulations of non-axisymmetric patterns in Taylor–Couette flow of dilute polymer solutions. *J. Non-Newtonian Fluid Mech.* **138**, 111–133.

THOMAS, D.G., KHOMAMI, B. & SURESHKUMAR, R. 2006*b* Pattern formation in Taylor–Couette flow of dilute polymer solutions: dynamical simulations and mechanism. *Phys. Rev. Lett.* **97**, 054501.

THOMAS, D.G., KHOMAMI, B. & SURESHKUMAR, R. 2009 Nonlinear dynamics of viscoelastic Taylor–Couette flow: effect of elasticity on pattern selection, molecular conformation and drag. *J. Fluid Mech.* **620**, 353–382.

TOMS, B.A. 1948 Some observations on the flow of linear polymer solutions through straight tubes at large Reynolds numbers. In *Proceedings of the First International Congress on Rheology* (ed. J.M. Burgers), pp. 135–141. North Holland.

VIRK, P.S. 1975 Drag reduction fundamentals. *AIChE J.* **21**, 625–656.

WEI, T., KLINE, E.M., LEE, S.H.-K. & WOODRUFF, S. 1992 Görtler vortex formation at the inner cylinder in Taylor–Couette flow. *J. Fluid Mech.* **245**, 47–68.

XI, L. & GRAHAM, M.D. 2010 Turbulent drag reduction and multistage transitions in viscoelastic minimal flow units. *J. Fluid Mech.* **647**, 421–452.